Mechanism for Amplitude Alternans in Electrocardiograms and the Initiation of Spatiotemporal Chaos

Diandian Diana Chen,[1] Richard A. Gray,[2] Ilija Uzelac,[1] Conner Herndon,[1] and Flavio H. Fenton[1,*]
[1]School of Physics, Georgia Institute of Technology, 837 State Street NW, Atlanta, Georgia 30332, USA
[2]Food and Drug Administration, 10903 New Hampshire Avenue, Silver Spring, Maryland 20993-0002, USA
(Received 28 June 2016; revised manuscript received 21 November 2016; published 20 April 2017)

It is widely believed that one major life-threatening transition to chaotic fibrillation occurs via spiral-wave breakup that is preceded by spatiotemporal dispersion of refractoriness due to alternations in the duration of the cardiac action potential (AP). However, recent clinical and experimental evidence suggests that other characteristics of the AP may contribute to, and perhaps drive, this dangerous dynamical instability. To identify the relative roles of AP characteristics, we performed experiments in rabbit hearts under conditions to minimize AP duration dynamics which unmasked pronounced AP amplitude alternans just before the onset of fibrillation. We used a simplified ionic cell model to derive a return map and a stability condition that elucidates a novel underlying mechanism for AP alternans and spiral breakup. We found that inactivation of the sodium current is key to developing amplitude alternans and is directly connected to conduction block and initiation of arrhythmias. Simulations in 2D where AP amplitude alternation led to turbulence confirm our hypothesis.

DOI: 10.1103/PhysRevLett.118.168101

Introduction.—Many spatially extended oscillatory and excitable systems in biology, physics, and chemistry are known to exhibit spatiotemporal chaos [1–3], where complex-disordered signals in both time and space are often driven by defect-mediated turbulence of spiral waves that continuously generate and annihilate in an irregular fashion, i.e., spiral-wave breakup [4]. Spiral-wave dynamics play a fundamental role in the study of cardiac dynamics [2], as they are often the underlying drivers of deadly arrhythmias such as tachycardia and fibrillation [2,5–7].

Dynamically induced dispersion of refractoriness by a period-doubling bifurcation [8–10] in the duration of cardiac action potentials (APs) is considered to be the main substrate for spiral-wave breakup in the heart. The dispersion in AP repolarization resulting from cellular alternans in AP duration [Fig. 1(a)] has been linked to alternans in the global electrocardiogram signal recorded from the body surface (Fig. 3 of the Supplemental Material [11]), and so-called T-wave alternans has been suggested as a biomarker for arrhythmia risk and survival rates [15]. Furthermore, a theoretical mechanism for this cellular bifurcation relates the slope of the AP duration (APD) restitution function [i.e., APD as a function of the preceding recovery time, also known as diastolic interval (DI)] to APD alternans [16,17] at the cellular level and spiral breakup in tissue [18,19]. However, other mechanisms such as memory, calcium dynamics [20–22], regional increases in K^+ levels [23], and conduction velocity restitution [9,10,22] have been shown to enhance or suppress this bifurcation independent of APD restitution slope.

While T-wave alternans can lead to regions with complex dispersion of refractoriness [24], recent experiments suggest that it is not necessarily cellular alternans in AP *duration* but rather in AP *shape* [25] and AP *amplitude* [26] that is significant in generating conduction block and spiral breakup. Furthermore, there is evidence of amplitude alternans in the QRS segment (corresponding to AP depolarization) of the electrocardiogram preceding the initiation of supraventricular tachycardia and during narrow QRS tachycardia [27]. These alternations have been shown to be rate dependent, occurring

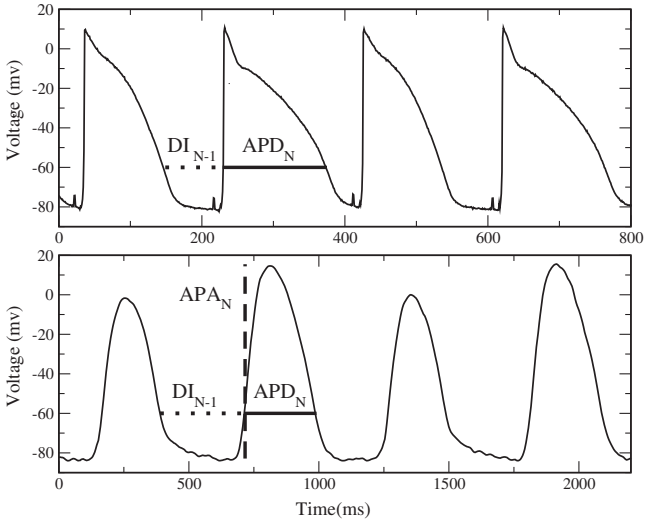

FIG. 1. Action potential alternans. (a) Endocardial microelectrode voltage signals from canine ventricles showing large alternans in APD (32 ms) but no alternans in APA. (b) Optical-mapping voltage signals from a pixel recorded from a rabbit ventricle surface perfused with low-calcium Tyrode's solution, low flow to simulate ischemia, and paced at a period of 550 ms. Horizontal dotted lines show measurement of DI, solid lines show measurement of APD, and the vertical dashed line APA.

only after an abrupt increase of rate above a critical value, and to be independent of the tachycardia mechanism [27]. This suggests a mechanism driven by cellular action potential amplitude (APA) alternans that is different from the one produced locally at small regions in between propagation and conduction block [24,28,29] (see Fig. 5 of the Supplemental Material [11]) due to electrotonic currents. Understanding the mechanism of rate-dependent QRS alternans could lead to important clinical implications. To our knowledge, there are no previous detailed studies linking cellular mechanisms of APA to tissue-level alternans of the QRS complex in the electrogram.

In this Letter we (1) demonstrate APA alternans in paced rabbit ventricles [Fig. 1(b)] using low-calcium Tyrode solution to minimize APD alternans that can mask other AP shape changes, (2) demonstrate that APA alternans are *not* due to conduction block (Figs. 3–5 of the Supplemental Material [11]), (3) propose simple mathematical ionic cell models that reproduce experimentally measured voltage dynamics (Fig. 1 of the Supplemental Material [11]), (4) derive a return map and corresponding analytical criterion for APA alternans (analogous to that for APD alternans [16,17]), (5) demonstrate that APA alternans can generate QRS amplitude alternans in a 1D cable when paced at fast rates, and (6) demonstrate that these APA alternans can lead to conduction block and produce spiral breakup with spatiotemporal patterns reminiscent of cardiac fibrillation. Our results implicate rapid inactivation of the rapid sodium current as a possible target for preventing APA alternans and the initiation of fibrillation.

Methods.—All experimental procedures were approved by the office of Research Integrity Assurance of Georgia Tech under IACUC no. A15034; see Supplemental Material for full details [11]. Briefly, rabbit hearts ($n = 5$) were optically mapped and voltage signals where recorded with normal and very low calcium Tyrode (62.5 μmol versus 2 mmol in normal) at pacing cycle lengths decreasing from 800 ms until fibrillation. In all cases, APA alternans appeared before the onset of fibrillation. For normal Tyrode, stable APD alternans (see Supplemental Material for definition [11]) was present for many cycle lengths with APA alternans appearing just before fibrillation. For low-Ca Tyrode no APD alternans was observed and only APA alternans developed before fibrillation; see Supplemental Material for more details [11].

APD map.—The APD restitution map is a fundamental tool in the analysis of cardiac dynamics as it relates each APD to its previous diastolic interval [16,17]:

$$\mathrm{APD}_{n+1} = R(\mathrm{DI}_n), \tag{1}$$

$$\mathrm{APD}_n + \mathrm{DI}_n = T(\mathrm{const}). \tag{2}$$

Similarly, we assume that APA is a function of the previous diastolic interval [as shown in Fig. 1(a)]. However, we further consider that the diastolic interval may be mapped to a state variable, the sodium inactivation recovery or h gate [30] [shown as a dashed line in Fig. 1(b) of the Supplemental Material [11]]. Therefore it is possible to find functions F and L such that

$$\mathrm{DI}_n = L(h_n), \tag{3}$$

$$\mathrm{APA}_{n+1} = F(h_n), \tag{4}$$

where h_n is the value of the sodium inactivation gate at the end of beat n. We also consider that APD is a function of the voltage's amplitude, $\mathrm{APD}_n = G(\mathrm{APA}_n)$, since the higher the maximum voltage amplitude, the longer the APD could be. Therefore, one can derive the relationship

$$T = G(\mathrm{APA}_n) + L(h_n). \tag{5}$$

These relationships are the building blocks of our APA map. From this foundation we derive below a stability condition for the fixed point of the system as a function of the sodium inactivation gate variable h and period T.

APA map.—We designate Eq. (4) as our APA restitution function. Then, Eq. (5) can be rearranged in the form

$$\mathrm{APA}_n = G^{-1}[T - L(h_n)] = Y(h_n, T), \tag{6}$$

which we designate as our APA period function. Note that both functions G and Y are considered to be decreasing monotonically.

Together, the APA period function $Y(h_n, T)$ and the APA restitution function $F(h_n)$ can be used to analyze the stability of the period-one response as a function of period T through linearization. To enhance understanding, we condensed the two functions into one return map by taking Eq. (6) and combining it with Eq. (4) by replacing the APA term in Eq. (4):

$$Y(h_{n+1}, T) = F(h_n). \tag{7}$$

We can rearrange this function to a return map form:

$$h_{n+1} = Y^{-1}(F(h_n), T). \tag{8}$$

Next, we linearize around h^*, where h^* is the fixed point, by having $h_n = h^* + \delta h_n$, then the stability condition for period-one cycling is given by

$$\left.\frac{\delta h_{n+1}}{\delta h_n}\right|_{h^*} = \left.\left(\frac{\delta Y^{-1}(F(h_n), T)}{\delta F(h_n)}\right)\left(\frac{\delta F(h_n)}{\delta h_n}\right)\right|_{h^*} = \frac{\frac{\delta F}{\delta h_n}|_{h^*}}{\frac{\delta Y}{\delta h_n}|_{h^*}}. \tag{9}$$

Thus, the stability condition becomes

$$1 \leq \left.\left|\frac{\text{slope of APA restitution function}}{\text{slope of period function}}\right|\right|_{h^*} \equiv |\rho|. \tag{10}$$

In other words, the ratio ρ of the slopes of the two functions determines the stability of the system's fixed point. If the condition in Eq. (10) is met, APA alternans may occur.

Simulations.—To investigate the applicability of the stability condition given by Eq. (10), we constructed a simplified ionic cell model of the form

$$\partial V/\partial t = D\partial^2 V/\partial x^2 - I_{\text{ion}},$$
$$dh/dt = (h_\infty - h)/\tau_h', \tag{11}$$

where V is the membrane voltage and h is the sodium inactivation gate. Since in the experiments very low calcium concentrations were used, we can assume to a first approximation that the calcium current is small enough to be neglected from the modeling. Therefore, we have that the I_{ion} in Eq. (11) consists of only two currents: one for sodium and one for potassium ($I_{\text{ion}} = I_{\text{Na}} + I_{\text{K}}$). The equations and values for I_{Na} and I_{K} for the model are given in the Supplemental Material [11].

Integration of Eq. (11) in single cells and in 1D leads to action potentials that match those obtained experimentally in the rabbit ventricles and Fig. 1 of the Supplemental Material [11]. Furthermore, the model can produce AP alternans. To validate the predictions of Eq. (10), we first numerically found the period for which alternans appears in the model by pacing the model in a single cell. The details of this protocol are in the Supplemental Material [11]. This was achieved at a period of around $T_C = 371$ ms with a critical h-gate value of $h_C = 0.450$. Next, while pacing the model faster, we measured the steady-state values of APD, DI, h-gate value, and APA as functions of T. From these values, we can extrapolate the restitution equation and the period equation [Eqs. (4) and (6), respectively]. Figure 2(a) shows the APA restitution function (solid line) for the model along with several period functions (dashed lines) calculated for different stimulation periods. The crossing of the period function and the restitution function is the fixed point of the system for that period. It can be noted that while for this model the APA restitution has a relatively smooth slope, the slope of the period functions, at the fixed points, increases in magnitude as the period increases. Therefore, according to Eq. (10), larger periods are more stable as their ρ value will have magnitudes $\ll 1$ agreeing with the numerical simulations. In fact, according to the map relation, the critical period at which the slope of the two curves combine to one, $T_C = 370.8$ ms and $h_C = 0.449$, closely matches the critical period obtained through pacing the numerical model. The maps in Fig. 2(b) show a cobweb diagram for two periods, one at 450 ms and another at 367 ms. The first period line shows a stable fixed point and the second shows alternans since the period is below the critical period.

The functionality and predictability of the single variable return map [Eq. (10)] can further be extended to an analytic stability condition by considering some approximations to the F, G, and L functions, giving then a better understanding of APA alternans development as a function of physiological parameters.

The following derivations are based on approximations of model behavior. Though cardiac dynamics is complex, we aim to gain intuitive understanding as a function of basic parameters and measurements; therefore, it would be desirable to have criteria in terms of physiological parameters.

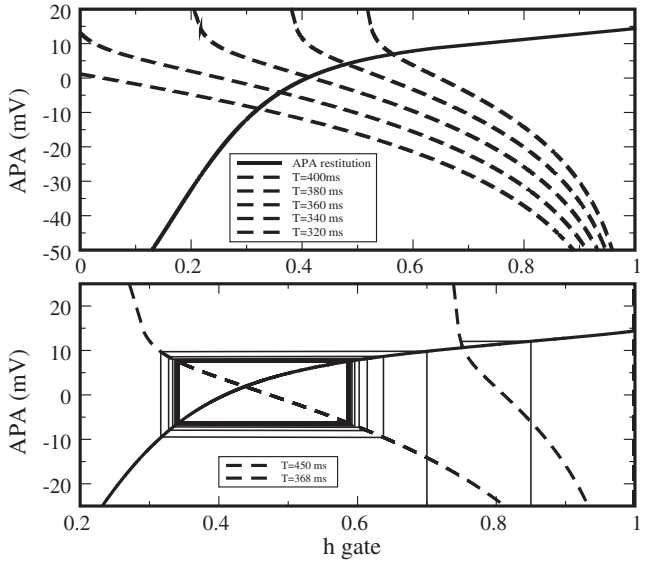

FIG. 2. Maps obtained for the numerical cell model. Top: Amplitude restitution curve as a function of the recovery of the h gate (solid line) and period curves (dashed lines) also as a function of h gate for five different periods (320, 340, 360, 380, and 400 ms). Bottom: Cobweb diagram for a period with a stable fixed point (450 ms dashed) and for a period with alternans (368 ms, solid line). Notice that the values for the h gate are bounded between 0 (closed) and 1 (fully open) and the APA alternates between -8 and 8 mV.

For example, the h gate for most cardiac cell models [31] follows an equation of the form given by Eq. (11), which leads to a recovery of inactivation that could be approximated by an exponential

$$h_n = 1 - ae^{-\text{DI}_n/\tau_h}. \tag{12}$$

Furthermore, if we consider that the APD is proportional to the APA, that is,

$$\text{APD}_n = \alpha \text{APA}_n + C_1, \tag{13}$$

then a constant stimulation period can be given by

$$\begin{aligned} T &= \text{APD}_n + \text{DI}_n \\ &= \alpha \text{APA}_n + C_1 - \tau_h[\ln(1 - h_n) - \ln(a)]. \end{aligned} \tag{14}$$

If we further consider that to first approximation the APA is linear with respect to the recovery variable h, then

$$\text{APA}_{n+1} = \beta h_n + B_1. \tag{15}$$

Then the 1D map stability condition given by Eq. (10) may be written as

$$\rho = \beta\alpha(h^* - 1)/\tau_h. \tag{16}$$

Note that we have dropped the absolute value bracket around ρ as the value of ρ is generally negative. This equation gives the guidelines for parameter values that can lead to APA alternans given simple numerical models. For example, the

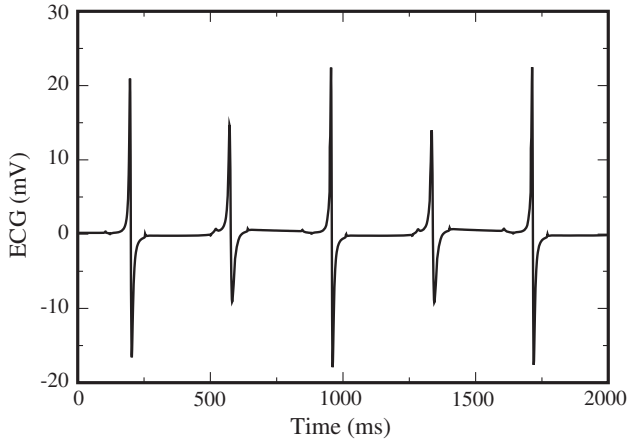

FIG. 3. Pseudo-Electrocardiogram showing pronounced QRS (sharp peaks) alternans from a 1D cable of length 200 cells using the model after pacing four times as in Fig. 1 of the Supplemental Material [11]. Note that since there is little change in APD, T-wave alternans is not very pronounced [34].

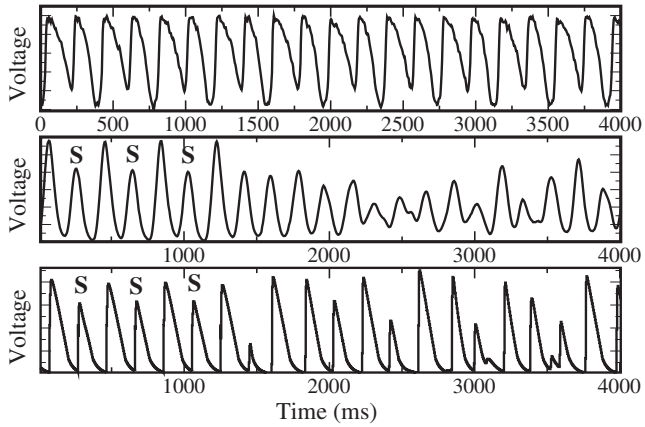

FIG. 4. Top: Optical-mapping voltage signal from one pixel from a rabbit heart with normal Tyrode paced at a fast period showing large APD alternans that is stable. Middle: Similarly, signal from one pixel from rabbit ventricle with low-calcium Tyrode and during APA alternans just before initiation of fibrillation. Bottom: Numerical model's voltage signal, in 2D, showing APA alternans before conduction block and initiation of arrhythmia.

parameters β, α, and τ_h are directly linked to the parameters g_{na}, I_k, and $\tau_{h'}$, respectively, in the model. Note that h^* depends on T, β, τ_h, and α through Eqs. (12)–(15). To validate the predictions of Eq. (16) a fit was made to Eqs. (12), (13), and (15) using the model. This results in $\alpha = 262.7$, $\beta = 0.5371$, and $\tau_h = 80$. Using these values in the analytic Eq. (16) it is possible to obtain ρ as a function of period and/or h^*. Here, our critical h_C value is 0.433 and critical T_C value is 366.25 ms when ρ is equal to -1. This critical value matches closely the h_C obtained by the map functions (0.449 for h_C and 370.8 ms for T_C) and by pacing the numerical simulations of the cell model (0.450 for h_C and 371 ms for T_C) shown before. To further validate the predictions of Eq. (16) we varied parameters in the model to modify the periods at which the model can generate APA alternans. As τ_h is multiplied with a factor from 0.5 to 2, the critical T_C changes from 355.5 to 387.5 ms, as shown in Fig. 2 of the Supplemental Material [11]. Furthermore, when τ_h is very large, the system can no longer produce APA alternans.

Numerical simulations of the model in a cable paced at fast rates showed that when APA alternans appeared, the calculated electrocardiogram results in QRS alternans, as shown in Fig. 3, similar to those observed in experiments and in the clinic [32,33]. More importantly, simulations in 2D demonstrated that while APD alternans can be very large, no conduction block was present; however, as APA developed, then conduction block was possible, as very small amplitudes will fail to propagate and will initiate spiral waves. This is consistent with our rabbit experiments, Figure 4, top, shows the voltage trace from an optical-mapping signal in a rabbit ventricle during fast pacing with very large APD alternans, and while dispersion is large, the dynamics is stable during the whole episode of several minutes of pacing. In contrast, Fig. 4, middle, shows that once large alternans in amplitude appeared, fibrillation could appear, just as in our 2D numerical simulations, as shown in Fig. 4, bottom.

Discussion.—Alternans as a mechanism for arrhythmias has historically been dominated by studies focused on contraction alternans [35] and T-wave alternans [8–10,24]. A few recent studies have shown that QRS alternans may be yet another mechanism for arrhythmia, particularly during narrow QRS tachycardias [27,36], where alternans has been shown to be a rate-related phenomenon that depends on an abrupt increase in rate activation above a critical frequency. Here, we derived a map and an analytic condition for when APA alternans can be expected at a cellular level and verified it with a numerical model. The numerical model showed that when paced in tissue at fast cycle lengths, it produces APA alternans in a single cell and resulted in conduction block in space. Recently, Myles *et al.* [26] showed that cellular alternans of action potential amplitude is notably present in rabbit hearts with heart failure and that APA is of particular importance in the initiation of ventricular fibrillation, and, in fact, more important than APD alternans [26,37]. They showed that post-infarction hearts are more vulnerable to ventricular arrhythmias at rapid rates and that APA alternans were associated with conduction block and ventricular fibrillation. Similarly, clinical data [25] have indicated that APA is more important in the development of arrhythmias in heart-failure patients, and APA was suggested to be the mechanism for T-wave alternans rather than APD. Furthermore, several experimental studies have shown that it is possible to sustain large gradients of APD alternans [5,8], even with several discordant alternans regions [24,38] that are stable (i.e., nodal lines do not move) and without conduction blocks, and still have no APA alternans. However, as the period is further decreased, then the development of APA discordant alternans has been shown to appear [9,26]. This can be linked to when the conduction velocity restitution starts to decrease in value [9], as there is a well-known correlation between conduction velocity and APA [39]. Our experimental

and numerical simulations agree with these previous results and show that it is possible to sustain large alternans in APD without the development of conduction block. This is because as long as the short APD can still preserve large amplitudes, it will be able to propagate. However, once APA develops, a very short APA will be unable to propagate.

In this Letter we linked cellular APA alternans to QRS alternans in the Electrocardiogram and created a framework to characterize when a given model will display APA alternans. A major conclusion of our analysis is the importance of sodium current in the dynamics of APA alternans. We have used a simple 1D map, analogous to the APD restitution map but for APA, that leads to an APA alternans condition given by Eq. (10). Cobweb diagrams of these maps show that indeed APA alternans will develop when parameters of the maps satisfy the criteria. We have also introduced a simple cell model that can produce alternans in APA and showed that a map reconstructed from the model agrees with the condition. Furthermore, by using simplified functions to describe the dynamics of the system, we have derived a simple analytic expression given by Eq. (10) that predicts alternans as a function of physiological model parameters, as shown in Eq. (16).

The simulations of the model equation in 1D and 2D show that APA alternans can lead to conduction block resulting in initiation of spiral waves and complex dynamics as observed experimentally. Our main result is that amplitude alternans-induced conduction block leading to spiral breakup can occur via inactivation of the sodium channel (that is, how quickly sodium channels fully recover). The analysis of the conditions for alternans indicates that sodium excitability, potassium, and the h-gate recovery are key to development, while calcium may be more important in the development of APD alternans. Our results suggest that targeting sodium-current inactivation dynamics (in addition to repolarization kinetics that generate APD alternans) should be considered as possible antiarrhythmic strategies.

This work was made possible by NSF Grants No. CNS-1347015 and No. CNS-1446675, AHA Grant No. 15POST25700285. F. H. F. would also like to thank NIMBioS (http://www.nimbios.org/workinggroups/WG_arrhythmias) Working Group on 'prediction and control of cardiac alternans' for useful discussions.

*Corresponding author.
flavio.fenton@physics.gatech.edu

[1] A. Goryachev and R. Kapral, Phys. Rev. Lett. **76**, 1619 (1996).
[2] G. Bub, A. Shrier, and L. Glass, Phys. Rev. Lett. **88**, 058101 (2002).
[3] S. W. Morris, E. Bodenschatz, D. S. Cannell, and G. Ahlers, Phys. Rev. Lett. **71**, 2026 (1993).
[4] M. C. Cross and P. C. Hohenberg, Science **263**, 1569 (1994).
[5] E. M. Cherry and F. H. Fenton, New J. Phys. **10**, 125016 (2008).
[6] R. A. Gray, J. Jalife, A. Panfilov, W. T. Baxter, C. Cabo, J. M. Davidenko, and A. M. Pertsov, Circulation **91**, 2454 (1995).
[7] R. A. Gray, A. M. Pertsov, and J. Jalife, Nature (London) **392**, 75 (1998).
[8] J. M. Pastore, S. D. Girouard, K. R. Laurita, F. G. Akar, and D. S. Rosenbaum, Circulation **99**, 1385 (1999).
[9] M. A. Watanabe, F. H. Fenton, S. J. Evans, H. M. Hastings, and A. Karma, J. Cardiovasc. Electrophysiol. **12**, 196 (2001).
[10] Z. Qu, A. Garfinkel, P.-S. Chen, and J. N. Weiss, Circulation **102**, 1664 (2000).
[11] See Supplemental Material at http://link.aps.org/supplemental/10.1103/PhysRevLett.118.168101 for a) A detailed description of the experimental methods, b) The model parameters, c) The effects of changing model parameters on the criteria for amplitude alterans, and d) experimental proof of the validity of our amplitude alternans that we obtained from the rabbit hearts, which includes Refs. [12–14].
[12] B. Echebarria and A. Karma, Phys. Rev. Lett. **88**, 208101 (2002).
[13] F. H. Fenton *et al.*, J. Veterinary Cardiol. **10**, 87 (2008).
[14] W. H. Gaskell, Phil. Trans. R. Soc. London **173**, 993 (1882).
[15] D. S. Rosenbaum *et al.*, New England Journal of medicine medical progress series **330**, 235 (1994).
[16] J. B. Nolasco and R. W. Dahlen, J. Appl. Physiol. **25**, 191 (1968).
[17] M. R. Guevara *et al.*, Electrical alternans and period doubling bifurcations, in *Computers in Cardiology* (IEEE, New York, 1984), pp. 167–170.
[18] M. Courtemanche, Chaos **6**, 579 (1996).
[19] F. H. Fenton, E. M. Cherry, H. M. Hastings, and S. J. Evans, Chaos **12**, 852 (2002).
[20] E. G. Tolkacheva, D. G. Schaeffer, D. J. Gauthier, and W. Krassowska, Phys. Rev. E **67**, 031904 (2003).
[21] M. E. Díaz *et al.*, Circulat. Res. **94**, 650 (2004).
[22] E. M. Cherry and F. H. Fenton, Am. J. Physiol. Heart Circulat. Physiol. **286**, H2332 (2004).
[23] Veniamin Y. Sidorov *et al.*, Am. J. Physiol. Heart Circulat. Physiol. **301**, H209 (2011).
[24] A. Gizzi *et al.*, Frontiers in Physiology **4**, 1 (2013).
[25] S. M. Narayan *et al.*, J. Am. College Cardiol. **52**, 1782 (2008).
[26] R. C. Myles, F. L. Burton, S. M. Cobbe, and G. L. Smith, J. Mol. Cell. Cardiol. **50**, 510 (2011).
[27] F. Morady *et al.*, J. Am. College Cardiol. **9**, 489 (1987).
[28] H. Arce, A. Xu, H. González, and M. R. Guevara, Chaos **10**, 411 (2000).
[29] F. H. Fenton *et al.*, J. Veterinary Cardiol. **10**, 87 (2008).
[30] A. L. Hodgkin and A. F. Huxley, J. Physiol. **117**, 500 (1952).
[31] F. H. Fenton and E. M. Cherry, Scholarpedia **3**, 1868 (2008).
[32] I. Uzelac *et al.*, in *Proceedings of the 38th IEEE Conference on Engineering in Medicine and Biology Society (EMBC), 2016* (IEEE, New York, 2016), pp 3941–3944.
[33] K. Gima and Y. Rudy, Circulation Res. **90**, 889 (2002).
[34] A. Bueno-Orovio, E. M. Cherry, and F. H. Fenton, J. Theor. Biol. **253**, 544 (2008).
[35] B. Surawicz and C. Fisch, J. Am. College Cardiol. **20**, 483 (1992).
[36] Y. T. Tai *et al.*, Clinical Cardiol. **14**, 1003 (1991).
[37] I. Martisienė *et al.*, BioMed Res. Int. **2015**, 951704 (2015).
[38] S. Mironov, J. Jalife, and E. G. Tolkacheva, Circulation **118**, 17 (2008).
[39] Robin M Shaw and Y. Rudy, Circulation Res. **80**, 124 (1997).